This Accepted Manuscript has not been copyedited and formatted. The final version may differ from this version.

eNeuro

Research Article: New Research | Development

Development of local circuit connections to hilar mossy cells in the mouse dentate gyrus

Yulin Shi[1], Steven F. Grieco[1], Todd C. Holmes[2] and Xiangmin Xu[1,3,4]

[1]*Department of Anatomy and Neurobiology, School of Medicine, University of California, Irvine, CA 92697-1275*
[2]*Department of Physiology and Biophysics, University of California, Irvine, CA 92697- 4560*
[3]*Department of Biomedical Engineering, University of California, Irvine, CA 92697-2715*
[4]*Department of Microbiology and Molecular Genetics, University of California, Irvine, CA 92697-4025*

https://doi.org/10.1523/ENEURO.0370-18.2019

Received: 21 September 2018

Revised: 15 February 2019

Accepted: 22 February 2019

Published: 7 March 2019

Y.S., S.F.G., T.C.H., and X.X. designed research; Y.S. and X.X. performed research; Y.S., S.F.G., T.C.H., and X.X. analyzed data; Y.S., S.F.G., T.C.H., and X.X. wrote the paper; X.X. contributed unpublished reagents/analytic tools.

Funding: NIH
NS078434
MH105427

The authors declare no competing financial interests.

Y.S. and S.F.G. These authors contribute equally to this work.

Correspondence should be addressed toAddress all correspondence to: Dr. Xiangmin Xu at xiangmin.xu@uci.edu

Cite as: eNeuro 2019; 10.1523/ENEURO.0370-18.2019

Alerts: Sign up at www.eneuro.org/alerts to receive customized email alerts when the fully formatted version of this article is published.

Accepted manuscripts are peer-reviewed but have not been through the copyediting, formatting, or proofreading process.

Copyright © 2019 Shi et al.
This is an open-access article distributed under the terms of the Creative Commons Attribution 4.0 International license, which permits unrestricted use, distribution and reproduction in any medium provided that the original work is properly attributed.

eNeuro Accepted Manuscript

eNeuro Accepted Manuscript

1 **Development of local circuit connections to hilar mossy cells in the mouse dentate gyrus**
2
3 **Running title**: Circuit development of hilar mossy cells
4
5 Yulin Shi[1*], Steven F. Grieco[1*], Todd C. Holmes[2], Xiangmin Xu[1, 3, 4]

6 1. Department of Anatomy and Neurobiology, School of Medicine, University of California,
7 Irvine, CA 92697-1275
8 2. Department of Physiology and Biophysics, University of California, Irvine, CA 92697-
9 4560
10 3. Department of Biomedical Engineering, University of California, Irvine, CA 92697-2715
11 4. Department of Microbiology and Molecular Genetics, University of California, Irvine, CA
12 92697-4025

13 * These authors contribute equally to this work.
14
15 **Author contributions**
16 Y.S., S.F.G and X.X. performed experiments. Y.S. and S.F.G. analyzed the data and wrote the
17 paper. T.C. and X.X. designed the research and wrote the paper.
18
19 **[#]Address all correspondence to:**
20 Dr. Xiangmin Xu
21 Department of Anatomy and Neurobiology
22 School of Medicine
23 University of California, Irvine
24 Irvine, CA 92697-1275
25 Tel: (949) 824-0040
26 Fax: (949) 824-8549
27 Email: xiangmin.xu@uci.edu
28
29 **Key Words**: Hippocampus, synaptic connections, excitatory input, inhibitory input, development
30 **Pages**: 31
31 **Figures**: 6
32 **Tables**: 3
33 **Word Counts**: Abstract=247; Significance Statement=70; Introduction=569; Discussion=1,477
34
35 **Funding sources and acknowledgements**
36 This work was funded by US National Institutes of Health grant MH105427 and BRAIN Initiative
37 Grant, R01NS104897. This work was also made possible in part through access to the confocal
38 facility of the Optical Biology Shared Resource of the Cancer Center Support Grant (CA-62203)
39 at the University of California, Irvine.
40
41 **Statement of conflict of interests**
42 The authors declare no competing financial interests.
43

44

45

46

eNeuro Accepted Manuscript

47 **Abstract**

48 Hilar mossy cells in the dentate gyrus (DG) shape the firing and function of the
49 hippocampal circuit. However, the neural circuitry providing afferent input to mossy cells is
50 incompletely understood, and little is known about the development of these inputs. Thus, we
51 used whole-cell recording and laser scanning photostimulation (LSPS) to characterize the
52 developmental trajectory of local excitatory and inhibitory synaptic inputs to mossy cells in the
53 mouse hippocampus. Hilar mossy cells were targeted by visualizing non-red fluorescent cells in
54 the dentate hilus of GAD2-Cre; Ai9 mice, which expressed tdTomato in GAD+ neurons, and
55 were confirmed by post hoc morphological characterization. Our results show that at postnatal
56 days 6-7 (P6-7), mossy cells received more excitatory input from neurons in the proximal CA3
57 versus those in the DG. In contrast, at P13-14 and P21-28, the largest source of excitatory
58 input originated in DG cells, while the strength of CA3 and hilar inputs declined. A
59 developmental trend was also evident for inhibitory inputs. Overall inhibitory input at P6-7 was
60 weak, while inhibitory inputs from the DG cell layer and the hilus predominated at P13-14 and
61 P21-28. The strength of local DG excitation and inhibition to mossy cells peaked at P13-14 and
62 decreased slightly in older P21-28 mice. Together, these data provide new detailed information
63 on the development of local synaptic connectivity of mossy cells, and suggests mechanisms
64 through which developmental changes in local circuit inputs to hilar mossy cells shape their
65 physiology and vulnerability to injury during postnatal periods.

eNeuro Accepted Manuscript

66 **Significance statement**

67 Mossy cells of the dentate gyrus (DG) have been implicated in hippocampal circuits
68 regulating pattern separation, an important function attributed to the DG. However, physiological
69 inputs regulating mossy cell activity are incompletely understood. Here, we show that sources of
70 both excitatory and inhibitory inputs arise developmentally. Our results suggest that excitatory
71 inputs from the DG and local inhibitory inputs are well-positioned to powerfully sculpt receptive
72 fields in mature mossy cells.

eNeuro Accepted Manuscript

73 **Introduction**

74 Mossy cells are principal excitatory neurons in the dentate gyrus (DG) of the
75 hippocampal formation (Scharfman, 1995; Scharfman and Myers, 2012; Soriano and Frotscher,
76 1994). Mossy cells are of significant interest, as they are an important circuit element within the
77 DG, which has been implicated in mediating cognitive functions such as pattern separation
78 (Myers and Scharfman, 2011; Sass et al., 1992; Scharfman, 2007). In addition, mossy cells
79 have been proposed to play an important role in temporal lobe epilepsy, as selective loss of DG
80 neurons accompanies this disorder, and mossy cells appear to be among the neurons most
81 vulnerable to injury and cell death (Sloviter, 1987). Very recently, three studies functionally
82 characterized mossy cells, focusing particularly on *in vivo* firing properties distinguishing mossy
83 cells from granule cells, another major neuron type in the DG, during behavior (Danielson et al.,
84 2017; GoodSmith et al., 2017; Senzai and Buzsaki, 2017). Mossy cells fire frequently and
85 possess multiple place fields, while granule cells exhibit extremely sparse and selective firing
86 and the majority of these neurons possess a single place field. The new findings prompt
87 intriguing questions regarding mossy cell circuit connections and information flow within the DG
88 circuitry (Nakazawa, 2017a).

89 Anatomical circuit connections within the DG have received significant experimental
90 attention, with many studies focusing on the DG granule cells (Amaral, 1978; Buckmaster and
91 Schwartzkroin, 1994; Buckmaster et al., 1992; Buckmaster et al., 1996; Scharfman, 2007;
92 Scharfman and Bernstein, 2015; Scharfman and Myers, 2012). However, a detailed
93 understanding of the excitatory and inhibitory synaptic inputs to hilar mossy cells is still lacking.
94 Furthermore, little is known about the development of local circuit connections to mossy cells.
95 Our recent rabies tracing work supports that mossy cells are major local circuit integrators (Sun
96 et al., 2017), and exert feedback modulation of DG functioning. In addition, the evolution of
97 functional circuit connections is correlated to the development of the spatial representation
98 system in the rodent hippocampal formation (Langston et al., 2010). It is important to note that

eNeuro Accepted Manuscript

99 a rudimentary map of space is already present when young rat pups (2.5 weeks old) explore an
100 open environment outside their nest for the first time; grid and place cells continue to evolve,
101 with many grid cells not reaching adult-like formation until about 4 weeks of age (Langston et
102 al., 2010).Thus, characterizing the development of afferent inputs to mossy cells is instrumental
103 for understanding mossy cell place-specific firing properties, and their contributions to
104 hippocampal function.

105 In the present study, we use a laser scanning photostimulation (LSPS)-based approach
106 to map and compare synaptic inputs of mossy cells across postnatal development (at ages P6-
107 7, P13-14, and P21-28). LSPS combined with whole-cell recordings has been an effective
108 approach in elucidating cortical circuit organization, as it allows presynaptic inputs to single
109 neurons to be mapped with high resolution glutamate-uncaging across a large anatomical area
110 (Kuhlman et al., 2013; Sun et al., 2014; Xu et al., 2016a; Xu et al., 2010b). Using this
111 physiological mapping approach, we provide a quantitative assessment of the spatial
112 distribution and input strength of excitatory and inhibitory inputs to mossy cells across the DG
113 and CA3 areas. Our results provide a detailed characterization of the functional organization of
114 afferent inputs to mossy cells at different postnatal ages. These findings are relevant to
115 understanding the *in vivo* physiology and function of mossy cells, and will advance our
116 understanding of the role of mossy cells in both health and disease.

eNeuro Accepted Manuscript

117 **Materials and Methods**

118 Hippocampal slice preparations

119 Sixty double-transgenic Ai9-tdTomato (RRID:IMSR_JAX:007905) X GAD2-ires-Cre
120 (RRID:IMSR_JAX:010802) male and female mice were used in these experiments. All
121 experiments were conducted in accordance with procedures approved by the Institutional
122 Animal Care and Use Committee. We obtained 1–3 high-quality hippocampal horizontal slices
123 from each mouse in which the DG and CA3 structures were clearly visible. To prepare living
124 brain slices, animals of 3 different ages (postnatal days 6–7, 13-14, and 21-28) were deeply
125 anesthetized with Nembutal (>100 mg/kg IP), rapidly decapitated, and their brains removed.

126 Hippocampal slices (400 µm thick) were cut at an angle of 20–30° to the horizontal plane
127 to conserve intrahippocampal axonal projections (Kopanitsa et al., 2006) in well oxygenated
128 (95% O_2-5% CO_2), ice-cold sucrose-containing cutting solutions (85 mM NaCl, 75 mM sucrose,
129 2.5 mM KCl, 25 mM glucose, 1.25 mM NaH_2PO_4, 4 mM $MgCl_2$, 0.5 mM $CaCl_2$, and
130 24 mM $NaHCO_3$). Slices were incubated for at least 30 minutes in sucrose-containing ACSF at
131 32°C before being transferred into slice-recording chambers with standard ACSF
132 (126 mM NaCl, 2.5 mM KCl, 26 mM $NaHCO_3$, 2 mM $CaCl_2$, 2 mM $MgCl_2$, 1.25 mM NaH_2PO_4,
133 and 10 mM glucose). Throughout cutting, incubation, and recording, ACSF was continuously
134 supplied with 95% O_2–5% CO_2.

135

136 Electrophysiology and laser-scanning photostimulation

137 We have previously described our methods for electrophysiological recording, imaging,
138 and photostimulation in detail, including the definitions of all reported parameters (Xu et al.,
139 2010a; Xu et al., 2006). For our more recent publications using these same methods see,
140 (Kuhlman et al., 2013; Sun et al., 2014; Xu et al., 2016a; Xu et al., 2010b). Briefly, whole-cell
141 recordings were performed in oxygenated ACSF at room temperature under a differential
142 interference contrast (DIC)/fluorescent Olympus microscope (BX51WI). ACSF was fed into the

eNeuro Accepted Manuscript

143 slice recording chamber through a custom-designed flow system driven by pressurized 95% O_2–
144 5% CO_2 (3 PSI) with a perfusion flow rate of about 2 mL/minute. Slices were first carefully
145 examined under a 4x objective to target the DG using visual landmarks (Amaral, 1978). To
146 perform whole-cell recordings, neurons were visualized at high magnification (60x objective, 0.9
147 NA; LUMPlanFl/IR, Olympus America Inc). Mossy cells targeted for recording were at least 50
148 µm below the surface of the slice and were initially identified based on the multipolar
149 appearance of the cell soma and presence of a thick apical dendrite, and later with fluorescent
150 imaging confirming the absence of GAD expression (Fig 1). Patch pipettes (4–6 MΩ resistance)
151 made of borosilicate glass were filled with an internal solution containing 126 mM K-gluconate, 4
152 mM KCl, 10 mM HEPES, 4 mM ATP-Mg, 0.3 mM GTP-Na, and 10 mM phosphocreatine (pH
153 7.2, 300 mOsm) when measuring excitatory postsynaptic currents (EPSCs) and action
154 potentials (APs). No correction was made for the liquid junction potential. Once the glass
155 pipette formed a gigaohm (GΩ) seal with the recorded cell membrane, the capacitance
156 compensation function of the Multiclamp 700B was used for automatic compensations of cell
157 membrane capacitance. In separate experiments, a cesium-based internal solution containing
158 130 mM CsOH, 130 mM D-gluconic acid, 0.2 mM EGTA, 2 mM $MgCl_2$, 6 mM CsCl, 10 mM
159 HEPES, 2.5 mM ATP-Na, 0.5 mM GTP-Na, and 10 mM phosphocreatine (pH 7.2, 300 mOsm)
160 was used to voltage clamp pyramidal neurons at the excitatory reversal potential (0–5mV) and
161 measure inhibitory postsynaptic currents (IPSCs). Electrodes also contained 0.1% biocytin for
162 posthoc anatomical cell labeling. Once stable whole-cell recordings were achieved with good
163 access resistance (usually ~ 30 MΩ), basic electrophysiological properties were characterized
164 using hyperpolarizing and depolarizing current injections. Electrophysiological data were
165 acquired with a Multiclamp 700B amplifier (Molecular Devices), data acquisition boards (models
166 PCI MIO 16E-4 and 6713, National Instruments), and a custom-modified version of Ephus
167 software 5 (Ephus, available at https://openwiki.janelia.org/). Data were digitized at 10 kHz and
168 stored on a computer.

eNeuro Accepted Manuscript

169 During photostimulation experiments, the microscope objective was switched from 60x
170 to 4x for LSPS. The same low-power objective lens was used for delivering ultraviolet flash
171 stimuli. Stock solution of MNI-caged-l-glutamate (Tocris Bioscience) was added to 20 mL of
172 circulating ACSF for a concentration of 0.2 mM caged glutamate. Hippocampal slice images
173 were acquired using the 4x objective with a high-resolution digital CCD camera, which in turn
174 was used for guiding and registering photostimulation sites. A laser unit (DPSS Lasers) was
175 used to generate 355 nm UV laser pulses for glutamate uncaging. Short pulses of laser flashes
176 (1 ms, 20 mW) were delivered using an electro-optical modulator and a mechanical shutter. The
177 laser beam formed uncaging spots, each approximating a Gaussian profile with a width of 100
178 µm in the focal plane.

179 As in previous studies, whole-cell recording of a single neuron was accompanied by
180 laser stimulation at nearby sites, generating action potentials from neurons in targeted areas via
181 LSPS-guided glutamate uncaging (Kuhlman et al., 2013; Sun et al., 2016; Xu et al., 2016a).
182 Voltage clamping the recorded neuron allowed determination of sites contributing synaptic input
183 (Fig. 3). By systematically surveying synaptic inputs from hundreds of different sites across a
184 large region, aggregate synaptic input maps were generated for individual neurons. For our
185 mapping experiments, a standard stimulus grid (12×12 stimulation sites covering an area of 500
186 X 600 µm) was used to survey synaptic input arising from hippocampal regions of interest,
187 including the DG, hilus, CA3, and CA1 (Fig 3A). The LSPS site spacing was empirically
188 determined to separate adjacent stimulation sites by the smallest predicted distance in which
189 photostimulation differentially activated adjacent neurons. Glutamate uncaging laser pulses
190 were delivered sequentially in a nonraster, nonrandom sequence, following a "shifting-X" pattern
191 designed to avoid revisiting the vicinity of recently stimulated sites (Shepherd et al., 2003).
192 Because glutamate uncaging agnostically activates both excitatory and inhibitory neurons, we
193 empirically determined the excitatory and inhibitory reversal potentials in mossy cells to isolate

eNeuro Accepted Manuscript

194 EPSCs and IPSCs. We voltage clamped the targeted cells at −70 mV to detect EPSCs, and use
195 the holding potential (0–5 mV) for IPSC detection with the cesium-containing internal solution.
196 Photostimulation data analysis has been described in detail (Shi et al., 2010; Sun et al.,
197 2016). Also see Figure 3. Responses occurring within the 10-ms window from laser onset are
198 considered direct. Synaptic currents with such short latencies are not possible because they
199 occur before the generation of action potentials in photostimulated neurons. Therefore, direct
200 responses are excluded from synaptic input analysis. It is possible that smaller synaptic
201 responses could be masked by direct glutamate responses. However, at some locations,
202 synaptic responses were over-riding on the relatively small direct responses and were identified
203 and included in synaptic input analysis. The input value of each stimulation site was measured
204 by the temporal summation (i.e., area under a curve) of individual EPSCs or IPSCs from each
205 photostimulation site with the baseline spontaneous response subtracted, and then normalized
206 by the analysis window of 150 ms after photostimulation. While the value actually represents
207 synaptic charge, for consistency with previous studies and because synaptic current is a more
208 familiar unit, this average integrated value is expressed in picoamperes (pA). As for individual
209 map construction, input measurements from different stimulation sites were assigned to their
210 corresponding anatomical locations in the hippocampus; color-coded maps of average input
211 amplitude and the number of events per site were plotted to illustrate overall input patterns to
212 the recorded cell.
213 To quantitatively compare input strengths and patterns across cell groups, we summed
214 the ESPC/IPSC input amplitudes and the numbers of EPSCs/IPSCs within and across specific
215 hippocampal subfields for individual cells. These measurements are termed the summed or
216 total input (excitation / inhibition) and the summed or total numbers of EPSCs/IPSCs of each
217 cell. We also performed analysis of EPSC/IPSC characteristics including their rise time, time
218 constant, and onset latency.
219

eNeuro Accepted Manuscript

220 Morphological examination and cell-type identification

221 After electrophysiological recording, brain slices were fixed in 4% paraformaldehyde
222 overnight, then transferred to 30% sucrose solution in PBS. Slices were stained against biocytin
223 with 1:500 Alexa Fluor 488-conjugated streptavidin (Jackson ImmunoResearch) to visualize the
224 morphology of recorded cells. Slices were also stained for 4′-6-diamidino-2-phenylindole (DAPI)
225 (Sigma-Aldrich) to identify laminar boundaries. Cell morphology was visualized using Olympus
226 BX 61 epifluorescent microscopy and the MetaMorph imaging suite (Molecular Devices).

227

228 Experimental Design and Statistical Analysis

229 Data are reported as mean values ± standard error of the mean (SEM). All statistical
230 analyses were performed using GraphPad Prism version 7.00 for Windows (GraphPad
231 Software, La Jolla California USA, www.graphpad.com”). For statistical comparisons between
232 groups, data were checked for normality and equal variance. For statistical comparisons across
233 the three developmental ages, we used the Kruskal–Wallis test (a non-parametric 1-way
234 ANOVA). Mann–Whitney U-tests and 1-way ANOVAs with Tukey’s post-hoc tests were used for
235 direct comparisons of groups. In all experiments, the level of statistical significance was defined
236 as $p < 0.05$.

237

238 **Results**

239 Development changes in intrinsic physiological properties of hilar mossy cells

240 Currently, there are no transgenic methods for directly distinguishing mossy cells from
241 other hilar neurons. Therefore, we use GAD2-Cre; Ai9 mice to facilitate mossy cell identification
242 and recording. In these mice, non-mossy cell inhibitory neurons (GAD-expressing) are
243 fluorescently labeled. Using a 60x objective, excitatory mossy cells are targeted for recording.
244 These neurons appeared as shadowed cell bodies, surrounded by fluorescently labeled GAD-

eNeuro Accepted Manuscript

245 expressing inhibitory neurons (Fig 1B). Biocytin infusion during whole-cell recording and post-
246 hoc staining was used to identify all mossy cells based on morphology (Fig 1C). The identity of
247 mossy cells could be verified by their characteristic regular-adapting spiking patterns in
248 response to suprathreshold current injection when the K+ containing internal solution was used
249 for electrical recordings (Fig 1D).

250 Intrinsic physiological properties of each recorded neuron were acquired immediately
251 after successful break-in with the recording electrode of the K+ containing internal solution.
252 Significant differences in physiological property measures were found in comparing the three
253 developmental age groups studied (P6-7, P13-14, P21-28) (Fig 2a, D). Input resistance,
254 measured with the membrane voltage change by hyperpolarizing current injection during whole
255 cell recording, (Rinput, in the unit of MΩ) declined with increasing age (Table 1). The Rinput of
256 P6-7 mossy cells was significantly larger than that of P13-14 and P21-28 neurons ($p = 0.02$ and
257 $p = 0.008$, respectively). The average R input of P6-7 mossy cells (N=11) was 637.7 ± 74 vs
258 439.8 ± 37.7in P13-14 mossy cells (N=12) and 341.7 ± 63.5 in P21-28 (N=13) mossy cells.
259 Monotonically declining Rinput values could result from increased conductance of ion channels,
260 or increased ion channel number in the cell membrane. Membrane capacitance (Cm) increased
261 in older animals, with significantly lower values present in the P6-7 group (Table 1; $p = 0.02$ and
262 $p = 0.08$ vs P13-14 and P21-28, respectively). However, resting membrane potential (RMP) did
263 not change significantly across developmental ages.

eNeuro Accepted Manuscript

264 After recording, neurons were immunostained with biocytin and cell morphology was
265 recovered using confocal imaging (Fig 2B,C). Young neurons (P6-7) had relatively smooth
266 proximal dendrites while dendrites in older animals (P13-P14 and P21-28) had many thorny
267 excrescences that were confined to the hilus. These morphological changes are consistent
268 with changes in the membrane capacitance that is proportional to the cell surface area.
269 Compared to smooth dendritic surfaces of mossy cells in young ages, the larger thorny surfaces
270 at older ages are correlated to larger cell membrane capacitance (see above). Further, thorny
271 excrescences are clusters of complex spines on proximal dendrites of mossy cells, which
272 indicate stronger synaptic connections between dentate granule cells and their postsynaptic
273 target neurons in older age groups. Thus these morphological changes are expected to be
274 correlated with stronger excitatory inputs from dentate granule cells to mossy cells in older ages
275 (see below).
276
277 Temporal precision of laser scanning photostimulation
278 LSPS can induce two major forms of responses: (1) direct activation of the recorded
279 neuron's glutamate receptors after glutamate uncaging; and (2) synaptically-mediated EPSCs or
280 IPSCs resulting from suprathreshold activation of presynaptic neurons. Excitatory responses
281 occurring within 10 ms after laser onset are caused by direct activation and exhibited larger
282 amplitudes and a distinct shape (longer rise time) occurring at short latencies after laser
283 stimulation (Fig 3C). Direct responses are excluded from local synaptic input analysis. However,
284 at some locations, synaptic responses are superimposed on relatively small direct responses
285 and were included in synaptic input analysis.
286 After each LSPS trial, we obtain a map of the raw signal traces (Fig 3B). A short
287 detection window (10–160ms after stimulation) is used to reduce the probability of detecting
288 spontaneous and polysynaptic events. Custom-written software (Shi et al., 2010) is used to
289 isolate the synaptically-mediated responses from direct responses and to calculate the average

290 amplitude, integrated input, event number, first event delay, rise time and decay constant of
291 each synaptic response. These quantitative data are turned into color-coded maps for further
292 region-specific analysis (Fig 3D–F). To reduce contamination by spontaneous events, we
293 average results from multiple photostimulation trials, and only anatomical sites with EPSCs or
294 IPSCs in all experiments are identified as presynaptic inputs. This temporally precise approach
295 shows that LSPS can be used for local circuit mapping of monosynaptic excitatory and inhibitory
296 connections to hilar mossy cells.
297
298 Spatial precision of laser scanning photostimulation
299 Prior to mapping synaptic inputs, we first characterize the spatial extent over which
300 neurons within the photostimulation area respond to laser pulses. We recorded from neurons in
301 the current clamp mode and examined action potentials elicited by photostimulating in the area
302 around the recorded neuron (Fig 4). The stimulation pattern is typically an 8 X 8 grid centered
303 on the recorded neuron, with width and length dimensions that ranged from 75 μm to 100 μm,
304 depending on the age of the slice. Generally, photostimulation proximal to the clamped neuron
305 is required to elicit action potentials. Across the developmental ages studied, the average
306 distance of photostimulation-evoked spikes from recorded cell bodies was 115.7 ± 12.7 μm
307 (N = 7 slices), 133.3 ± 26.7 μm (N=3), and 127.5 ± 8.9 μm (N=12), for DG granule cells, hilar
308 neurons, and proximal CA3 cells, respectively. Further, the excitability of the presynaptic
309 sources that is measured by the average number of evoked spikes per cells did not differ
310 significantly across the age groups. These data show that LSPS can be used for local circuit
311 mapping of monosynaptic excitatory and inhibitory connections to hilar mossy cells.
312
313 Excitatory synaptic inputs to mossy cells
314 A total of 31 mossy cells were recorded from hippocampal slices taken from P6-7, P13-
315 14, and P21-28 mice (Fig 5; N = 12, 9, and 10 neurons, respectively). The amplitude of summed

eNeuro Accepted Manuscript

eNeuro Accepted Manuscript

316 excitatory inputs, excitatory inputs from multiple neurons averaged (see (Shi et al., 2010; Sun et
317 al., 2014; Xu et al., 2016b)), from the DG was weak in P6-7 mice, and significantly increased in
318 P13-14 and P21-28 mice (Fig 5A, 5C-D). Although the excitation from the DG declined slightly
319 at P21-28, this was not a statistically significant change (vs P13-14 mice). We found that mossy
320 cells at P6-7 receive a majority of their excitatory inputs from the CA3 (Fig 5C, right panel, and
321 Figure 5D), indicating the presence of a strong CA3 backprojection. As development proceeded,
322 the strength of CA3 and hilar inputs diminished and mossy cells received more of their
323 excitatory input from the DG (Fig 5C-D). Consistent with summed input measurements,
324 recorded cells received average integrated excitatory input of 44.8 ± 8.4 pA from the DG at P6-
325 7; 189.9 ± 59.0 pA at P13-14; and 105.9 ± 12.4 pA at P21-28. The DG input constituted 29.1% ±
326 6.1% of the total excitation received by mossy cells at P6-7, 62.7% ± 6.2% at P13-14, and
327 72.2% ± 7.1% at P21-28. The per stimulation site input also increased from 3.6 ± 0.5 pA at P6-7
328 to 9.6 ± 1.5 pA and 8.3 ± 1.3 pA at P13-14 and P21-28, respectively (Table 2A).

329 Relative to the input from the DG, the CA3 provided more input at P6-7 and much less
330 input at P13-14 and P21-28 (Fig. 5C-D). The integrated input from CA3 was 73.1± 19.9 pA at
331 P6-7, 43.7 ± 14.6 pA at P13-14 and 20.7 ± 7.9 pA at P21-28. Input from the hilus followed a
332 similar pattern. The integrated input from the hilus was 18.8 ± 4.6 pA at P6-7, 10.9 ± 6.6 pA at
333 P13-14 and 5.3 ± 2.5 pA at P21-28. The average percent of evoked excitatory inputs from the
334 hilus was 18.2% ± 6.3%, 4.8% ± 1.7%, and 3.6% ± 1.7% for P6-7, P13-14, and P21-28,
335 respectively. The per-stimulation site input decreased from 4.1 ± 1.0 pA at P7 to 3.1 ± 1.3 pA
336 and 1.4 ± 0.5 pA at P13-14 and P21-28, respectively (Table 2A).

337 The event frequency, which represents the number of evoked synaptic events per
338 second to a recorded neuron was also measured (Fig 5B). The number of EPSCs evoked per
339 DG stimulation site was 3.2 ± 0.5, 3.9 ± 0.4, and 3.4 ± 0.1 in P6-7, P13-14, and P21-P28 mice,
340 respectively. The number of evoked EPSCs per hilar stimulation site was 3.3 ± 0.6, 1.7 ± 0.5,
341 and 0 ± 00 in P6-7, P13-14, and P21-28 groups, respectively. The number of EPSCs evoked

eNeuro Accepted Manuscript

342 per CA3 stimulation site was 3.4 ± 0.4, 2.4 ± 0.3, and 1.7 ± 0.3 in P6-7, P13-14, and P21-P28
343 groups, respectively. The average latencies of EPSCs did not differ significantly between the
344 three age groups (Table 2B).

345 We calculated the number of input locations activated as a DG/CA3 connectivity ratio
346 and found that the ratio for EPSCs trends very strongly (P=.0539; Kruskal-Wallis test) towards
347 increasing from p6-7 to p21-28 supporting our hypothesis that excitatory inputs shift to the DG
348 by the end of development. We also analyzed the distances of recorded mossy cells to the DG
349 and CA3 and confirmed that systemic differences between age groups did not account for our
350 results.

351

352 Inhibitory synaptic inputs to mossy cells

353 A total of 33 mossy cells were recorded from P6-7, P13-14, and P21-28 mice (Fig 6;
354 N=10, 7, and 16). Based on region specific-analysis of inhibitory input sources, we found that at
355 P6-7, mossy cells received roughly equivalent inhibitory input from the DG, hilus, and CA3 (Fig
356 6A, 6C). As mice aged, inhibition from the DG and CA3 peaked at P13-P14 and then decreased
357 at older ages (P21-28; Fig 6C-D). The amplitude of inhibitory input from the DG was significantly
358 larger than that from the CA3. The magnitude of hilar inhibition did not significantly change over
359 the course of development. Mossy cells received 68.5 ± 24.0 pA of integrated inhibitory input
360 from the DG at P6-7, 490.7 ± 100.6 pA at P13-14, and 195.7 ± 37.0 pA at P21-28. DG input
361 constituted 31.2% ± 6.1% of excitatory input at P6-7, 62.7% ± 6.2% at P13-14, and
362 64.9% ± 3.5% at P21-28. The magnitude of inhibition per stimulation site was 3.9 ± 0.9 pA,
363 12.8 ± 1.4 pA, and 6.6 ± 0.8 pA at P6-7, P13-14, and P21-28, respectively (Table 3A). The CA3
364 provided more inhibition at P13-14 and substantially less input at P6-7 and P21-28. Integrated
365 inhibitory input from CA3 neurons was 77.1 ± 20.5 pA at P6-7, 150.6 ± 30.4 pA at P13-14 and
366 51.7 ± 13.5 pA at P21-28. CA3 neurons provided 40.5% ± 6.2%, 18.5% ± 2.5% and
367 11.6% ± 2.9% of inhibitory input to mossy cells at P6-7, P13-14, and P21-28, respectively.

eNeuro Accepted Manuscript

368 Average inhibition per stimulation site was 4.3 ± 0.8 pA, 10.8 ± 2.1 pA, and 4.2 ± 0.5 pA at P6-7,
369 P13-14, and P21-28 (Table 3A).
370 Inhibitory input from the hilus was generally weak and diffuse across all ages studied.
371 Average integrated input was 28.1 ± 8.8 pA at P6-7, 132.2 ± 35.2 pA at P13-14, and
372 31.5 ± 4.7 pA at P21-28. Input from the hilus accounted for 18.2% ± 3.9%, 14.9% ± 2.9%, and
373 17.8% ± 4.5% of the inhibitory input to mossy cells. Input per stimulation site was 4.7 ± 1.3 pA,
374 10.7 ± 2.1 pA, and 4.7 ± 0.5 pA at P6-7, P13-14, and P21-28, respectively (Table 3A).
375 The frequency of LSPS-evoked IPSCs was also measured independently from IPSC
376 strength (Fig 6B). The number of evoked IPSCs per stimulation site in the DG was 2.0 ± 0.4,
377 3.7 ± 0.4, and 2.9 ± 0.2 at P6-7, P13-14, and P21-P28. The number of evoked IPSCs per
378 stimulation site in the hilus was 2.6 ± 0.6, 3.4 ± 0.6, and 2.6 ± 0.2 in P6-7, P13-14, and P21-28
379 mice, respectively. Finally, the number of evoked IPSCs per stimulation site in the CA3 was
380 2.2 ± 0.4, 3.0 ± 0.5 and 1.8 ± 0.3 in P6-7, P13-14, and P21-P28 mice (Table 3B).
381 There was a general trend for the latency of IPSC onset after photostimulation to
382 decrease from P6-7 to P13-14, and increase from P13-14 to P21-28. For DG-evoked IPSCs, the
383 latency to IPSC onset was significantly longer at P6-7 vs other ages, while the latency to IPSC
384 onset in P13-14 mice was significantly shorter than in P21-28 animals. For CA3-evoked IPSCs,
385 the latency to IPSC onset was significantly longer in P6-7 mice vs other ages. Differences in the
386 IPSC onset latency after hilar stimulation did not reach significance (Table 3C).
387 We calculated the number of input locations activated as a DG/CA3 connectivity ratio.
388 The DG/CA3 input number ratio for IPSCs increases from p6-7 to p21-28 and from p13-14 to
389 p21-28, also supporting our hypothesis that inhibitory inputs to mossy cells shift to the DG by
390 the end of development as well. We also analyzed the distances of recorded mossy cells to the
391 DG and CA3 to confirm that systemic differences between age groups did not account for our
392 results. A difference was only observed for calculated distances of IPSC map sites in CA3 and
393 mossy cells for p6-7 versus p21-28.

eNeuro Accepted Manuscript

394

395 **Discussion**

396 In the present study, LSPS combined with whole-cell patch clamping was used to
397 assess excitatory and inhibitory synaptic inputs to mossy cells over the course of postnatal
398 development in mice. Our study is the first to provide a comprehensive evaluation of the spatial
399 distribution and input strength of local circuit connections to mossy cells. Both excitatory and
400 inhibitory input to hilar mossy cells evolved dynamically over the course of development. At P6-
401 7, the majority of excitatory input to mossy cells came from CA3, with summed ESPC input that
402 nearly doubled that of input from the DG. Input from the hilus was modest. Within a week (at
403 P13-14), input from the DG had substantially increased (nearly a four-fold increase), while
404 excitatory inputs from both the CA3 and the hilus declined. Input from the DG remained the
405 strongest source of excitatory drive to mossy cells in young adulthood (P21-28).

406 A roughly similar pattern was apparent in the development of inhibitory input to mossy
407 cells. At the youngest postnatal age studied (P6-7), input from the CA3 predominated, with less
408 robust input from the DG. By P13-14, the relative strength of inhibitory input from these sources
409 reversed, with the strongest input from the DG. This balance of inhibitory input persisted through
410 young adulthood. Inhibitory input from the hilus was modest at all ages studied. For both
411 excitatory and inhibitory drive, summed input strength was relatively weak at early postnatal
412 ages, peaked at P13-14, and declined in early adulthood at P21-28.

413

414 Multiple inputs shape mossy cell physiology

415 Within the dentate gyrus, mossy cells, granule cells, and local interneurons display a
416 complex pattern of recurrent connectivity that has been implicated in pattern separation, an
417 important role of the DG. Recent studies have shown that the electrophysiological
418 characteristics of mossy cells differ greatly from those of granule cells (Danielson et al., 2017;
419 GoodSmith et al., 2017; Senzai and Buzsaki, 2017). While granule cells fire sparsely (at low

eNeuro Accepted Manuscript

420 frequency) and selectively and typically have only a single place field, mossy cells fire at higher
421 frequencies and more promiscuously, with multiple place fields. Moreover, mossy cells remap
422 place fields more rapidly when exposed to new environmental cues. Though mossy cells
423 receive strong, monosynaptic excitatory drive directly from granule cells, these studies found
424 that mossy cell firing was only rarely driven by granule cells with overlapping place fields,
425 suggesting excitatory drive creating place fields in mossy cells likely stems from other sources.
426 The sources of this input, important for understanding circuits underlying pattern separation,
427 remains undefined. CA3 pyramidal cells and dentate semilunar granule cells have been
428 proposed as candidate sources of input (Nakazawa, 2017b). There are reports of place field
429 representations developing into adulthood in hippocampus as well (Langston et al., 2010).
430 Indeed, while additional studies are needed to fully understand the contribution of dentate gyrus
431 and CA3 neurons to mossy cell place fields, CA3 excitatory inputs likely can contribute to
432 interesting mossy cell physiology *in vivo* as discussed above.
433 Our results show that while excitatory drive from CA3 provides the bulk of the excitatory
434 input to mossy cells in very young animals (P6-7), this is a developmentally transient state that
435 does not persist into adulthood. In the mature hippocampal circuit (in P21-28 mice), a majority
436 of the excitatory drive to mossy cells originates from neurons with cell bodies in the DG. It is
437 possible that semilunar granule neurons provide a defining excitatory input to hilar mossy cells,
438 as semilunar neurons are glutamatergic neurons in the inner molecular layer that provide mossy
439 cells with excitatory input creating persistent bursting activity (Larimer and Strowbridge, 2010).
440 Further investigation is required to determine how these neurons may contribute to receptive
441 field structure in mossy cells.
442
443 Comparison of excitatory and inhibitory inputs to mossy cells
444 Our experimental results confirm the finding that mossy cells receive strong excitatory
445 innervations from DG granule cells in the mature hippocampus. However, our results show for

eNeuro Accepted Manuscript

446 the first time that excitation from the DG is weak at P6-7 (Table 2A). This is consistent with the
447 finding that thorny excrescences appear only at rather late ages (around P9) and do not
448 become common until P14 in the rodent (Ribak et al., 1985). Young mossy cells (in P6-7 mice)
449 had most of their excitatory input from CA3, although the strength of this input decreased
450 significantly at later ages. Excitatory input from the hilus, which was overall weak at all ages
451 studied, could result from recurrent connections originating from other mossy cells.
452 Inhibition of mossy cells originated predominantly from synaptic inputs from the DG and
453 CA3. At the youngest ages studied, inhibition was relatively weak overall and came from DG,
454 hilar, and CA3 inputs. As animals aged, inhibition from the DG increased significantly, while
455 inhibition from the CA3 and hilus declined. Both excitation and inhibition from the DG peaked at
456 P14 and decreased slightly at P21-P28. Although further studies are necessary to reveal the
457 mechanism of this reduction, pruning of initially exuberant synaptic connections and decreases
458 in DG cell density could contribute to decreased mossy cell input (Sadgrove et al., 2006;
459 Seress, 1977).
460 Overall, local excitation and inhibition to mossy cells showed different developmental
461 trends. However, excitatory and inhibitory synaptic connectivity was broadly balanced across
462 local networks during each postnatal period studied.
463
464 Mossy cell development and formation of canonical trisynaptic circuits
465 The DG-CA3-CA1 trisynaptic circuit is considered a fundamental principle of neuronal
466 organization in the hippocampus. Cortical information enters the DG from the entorhinal cortex.
467 DG granule cells project to CA3 pyramidal neurons through mossy fibers (which also synapse
468 on local mossy cells). CA3 pyramidal neurons send Shaffer collaterals that synapse on CA1
469 pyramidal neurons (as well as forming local connections within the CA3). CA1 neurons then
470 send efferent connections back to the entorhinal cortex. Information flow through this circuit is
471 typically considered to be unidirectional in the mature hippocampus.

eNeuro Accepted Manuscript

472 However, exceptions to this unidirectional flow, particularly in the immature
473 hippocampus, have been documented. In a previous study we found that network activity
474 propagated bidirectionally through this circuit (Shi et al., 2014). Activity that originated in the
475 distal CA3 propagated towards the DG and CA1 at the same time in the young hippocampus (in
476 P1-14 mice). This propagation was mediated by AMPA receptors, and was developmentally
477 transient, gradually disappearing by P14.

478 It is not clear how this bidirectional propagation develops, nor how the flow of activity
479 becomes predominantly unidirectional in the mature hippocampal circuit. In past studies,
480 biocytin staining and paired recording have shown that axon collaterals of CA3 pyramidal
481 neurons directly innervate and activate mossy cells and GABAergic neurons (Scharfman, 1994)
482 in the dentate and hilus. These neurons in turn sends axons to the molecular layer targeting
483 granule cells. In the present study, we discovered that mossy cells received a relatively strong
484 excitatory backprojection from the CA3 at P6-7. The strength of this input declined at older
485 ages. While inhibitory input from CA3 also decreased over the course of development, the
486 latency to evoke inhibitory responses was faster than that for excitatory responses. Rapid onset
487 of inhibition in mossy cells could prevent these neurons from activating granule cells,
488 contributing to a unidirectional flow of information through the mature hippocampal circuit.

489 In addition to their potential roles in cognitive function mediated by the dentate gyrus,
490 hilar mossy cells are interesting due to their vulnerability to excitotoxicity in temporal lobe
491 epilepsy (Scharfman and Myers, 2012). Mossy cell loss has been observed both in humans with
492 temporal lobe epilepsy and in animal epilepsy models. The massive excitatory inputs from both
493 the DG and the CA3 could put mossy cells at risk of cell death during epileptic firing, when
494 levels of inhibitory input are chronically decreased. Indeed, in slice and *in vivo* recordings, we
495 and others have observed that mossy cells receive a great deal of excitatory drive from local
496 circuits via a continuous barrage of large spontaneous EPSPs (Buckmaster and Schwartzkroin,
497 1995; Scharfman, 1993; Scharfman and Schwartzkroin, 1988; Strowbridge and Schwartzkroin,

498 1996). Our present results suggest that robust excitatory drive from the DG in the mature

499 hippocampus may provide the afferent inputs that lead to excitotoxicity.

eNeuro Accepted Manuscript

500 **References**

501 Amaral, D.G. (1978). A Golgi study of cell types in the hilar region of the hippocampus in the
502 rat. J Comp Neurol *182*, 851-914.
503 Buckmaster, P.S., and Schwartzkroin, P.A. (1994). Hippocampal mossy cell function: a
504 speculative view. Hippocampus *4*, 393-402.
505 Buckmaster, P.S., and Schwartzkroin, P.A. (1995). Interneurons and inhibition in the dentate
506 gyrus of the rat in vivo. J Neurosci *15*, 774-789.
507 Buckmaster, P.S., Strowbridge, B.W., Kunkel, D.D., Schmiege, D.L., and Schwartzkroin, P.A.
508 (1992). Mossy cell axonal projections to the dentate gyrus molecular layer in the rat hippocampal
509 slice. Hippocampus *2*, 349-362.
510 Buckmaster, P.S., Wenzel, H.J., Kunkel, D.D., and Schwartzkroin, P.A. (1996). Axon arbors and
511 synaptic connections of hippocampal mossy cells in the rat in vivo. J Comp Neurol *366*, 271-
512 292.
513 Danielson, N.B., Turi, G.F., Ladow, M., Chavlis, S., Petrantonakis, P.C., Poirazi, P., and
514 Losonczy, A. (2017). In Vivo Imaging of Dentate Gyrus Mossy Cells in Behaving Mice. Neuron
515 *93*, 552-559 e554.
516 GoodSmith, D., Chen, X., Wang, C., Kim, S.H., Song, H., Burgalossi, A., Christian, K.M., and
517 Knierim, J.J. (2017). Spatial Representations of Granule Cells and Mossy Cells of the Dentate
518 Gyrus. Neuron *93*, 677-690 e675.
519 Kopanitsa, M.V., Afinowi, N.O., and Grant, S.G. (2006). Recording long-term potentiation of
520 synaptic transmission by three-dimensional multi-electrode arrays. BMC Neurosci *7*, 61.
521 Kuhlman, S.J., Olivas, N.D., Tring, E., Ikrar, T., Xu, X., and Trachtenberg, J.T. (2013). A
522 disinhibitory microcircuit initiates critical-period plasticity in the visual cortex. Nature *501*, 543-
523 546.
524 Langston, R.F., Stevenson, C.H., Wilson, C.L., Saunders, I., and Wood, E.R. (2010). The role of
525 hippocampal subregions in memory for stimulus associations. Behav Brain Res *215*, 275-291.
526 Larimer, P., and Strowbridge, B.W. (2010). Representing information in cell assemblies:
527 persistent activity mediated by semilunar granule cells. Nat Neurosci *13*, 213-222.
528 Myers, C.E., and Scharfman, H.E. (2011). Pattern separation in the dentate gyrus: a role for the
529 CA3 backprojection. Hippocampus *21*, 1190-1215.
530 Nakazawa, K. (2017a). Dentate Mossy Cell and Pattern Separation. Neuron *93*, 1236.
531 Nakazawa, K. (2017b). Dentate Mossy Cell and Pattern Separation. Neuron *93*, 465-467.
532 Ribak, C.E., Seress, L., and Amaral, D.G. (1985). The development, ultrastructure and synaptic
533 connections of the mossy cells of the dentate gyrus. J Neurocytol *14*, 835-857.
534 Sadgrove, M.P., Laskowski, A., and Gray, W.P. (2006). Examination of granule layer cell count,
535 cell density, and single-pulse BrdU incorporation in rat organotypic hippocampal slice cultures
536 with respect to culture medium, septotemporal position, and time in vitro. J Comp Neurol *497*,
537 397-415.
538 Sass, K.J., Sass, A., Westerveld, M., Lencz, T., Novelly, R.A., Kim, J.H., and Spencer, D.D.
539 (1992). Specificity in the correlation of verbal memory and hippocampal neuron loss:
540 dissociation of memory, language, and verbal intellectual ability. J Clin Exp Neuropsychol *14*,
541 662-672.
542 Scharfman, H.E. (1993). Characteristics of spontaneous and evoked EPSPs recorded from
543 dentate spiny hilar cells in rat hippocampal slices. J Neurophysiol *70*, 742-757.

eNeuro Accepted Manuscript

eNeuro Accepted Manuscript

544 Scharfman, H.E. (1994). Evidence from simultaneous intracellular recordings in rat hippocampal
545 slices that area CA3 pyramidal cells innervate dentate hilar mossy cells. J Neurophysiol *72*,
546 2167-2180.
547 Scharfman, H.E. (1995). Electrophysiological evidence that dentate hilar mossy cells are
548 excitatory and innervate both granule cells and interneurons. J Neurophysiol *74*, 179-194.
549 Scharfman, H.E. (2007). The CA3 "backprojection" to the dentate gyrus. Prog Brain Res *163*,
550 627-637.
551 Scharfman, H.E., and Bernstein, H.L. (2015). Potential implications of a monosynaptic pathway
552 from mossy cells to adult-born granule cells of the dentate gyrus. Front Syst Neurosci *9*, 112.
553 Scharfman, H.E., and Myers, C.E. (2012). Hilar mossy cells of the dentate gyrus: a historical
554 perspective. Front Neural Circuits *6*, 106.
555 Scharfman, H.E., and Schwartzkroin, P.A. (1988). Electrophysiology of morphologically
556 identified mossy cells of the dentate hilus recorded in guinea pig hippocampal slices. J Neurosci
557 *8*, 3812-3821.
558 Senzai, Y., and Buzsaki, G. (2017). Physiological Properties and Behavioral Correlates of
559 Hippocampal Granule Cells and Mossy Cells. Neuron *93*, 691-704 e695.
560 Seress, L. (1977). The postnatal development of rat dentate gyrus and the effect of early thyroid
561 hormone treatment. Anat Embryol (Berl) *151*, 335-339.
562 Shepherd, G.M., Pologruto, T.A., and Svoboda, K. (2003). Circuit analysis of experience-
563 dependent plasticity in the developing rat barrel cortex. Neuron *38*, 277-289.
564 Shi, Y., Ikrar, T., Olivas, N.D., and Xu, X. (2014). Bidirectional global spontaneous network
565 activity precedes the canonical unidirectional circuit organization in the developing
566 hippocampus. J Comp Neurol *522*, 2191-2208.
567 Shi, Y., Nenadic, Z., and Xu, X. (2010). Novel use of matched filtering for synaptic event
568 detection and extraction. PLoS One *5*, e15517.
569 Sloviter, R.S. (1987). Decreased hippocampal inhibition and a selective loss of interneurons in
570 experimental epilepsy. Science *235*, 73-76.
571 Soriano, E., and Frotscher, M. (1994). Mossy cells of the rat fascia dentata are glutamate-
572 immunoreactive. Hippocampus *4*, 65-69.
573 Strowbridge, B.W., and Schwartzkroin, P.A. (1996). Transient potentiation of spontaneous
574 EPSPs in rat mossy cells induced by depolarization of a single neurone. J Physiol *494 (Pt 2)*,
575 493-510.
576 Sun, Y., Grieco, S.F., Holmes, T.C., and Xu, X. (2017). Local and Long-Range Circuit
577 Connections to Hilar Mossy Cells in the Dentate Gyrus. eNeuro *4*.
578 Sun, Y., Ikrar, T., Davis, M.F., Gong, N., Zheng, X., Luo, Z.D., Lai, C., Mei, L., Holmes, T.C.,
579 Gandhi, S.P.*, et al.* (2016). Neuregulin-1/ErbB4 Signaling Regulates Visual Cortical Plasticity.
580 Neuron *92*, 160-173.
581 Sun, Y., Nguyen, A.Q., Nguyen, J.P., Le, L., Saur, D., Choi, J., Callaway, E.M., and Xu, X.
582 (2014). Cell-type-specific circuit connectivity of hippocampal CA1 revealed through Cre-
583 dependent rabies tracing. Cell Rep *7*, 269-280.
584 Xu, X., Olivas, N.D., Ikrar, T., Peng, T., Holmes, T.C., Nie, Q., and Shi, Y. (2016a). Primary
585 visual cortex shows laminar-specific and balanced circuit organization of excitatory and
586 inhibitory synaptic connectivity. J Physiol *594*, 1891-1910.
587 Xu, X., Olivas, N.D., Levi, R., Ikrar, T., and Nenadic, Z. (2010a). High precision and fast
588 functional mapping of cortical circuitry through a combination of voltage sensitive dye imaging
589 and laser scanning photostimulation. J Neurophysiol *103*, 2301-2312.

eNeuro Accepted Manuscript

590 Xu, X., Olivas, N.D., Levi, R., Ikrar, T., and Nenadic, Z. (2010b). High precision and fast
591 functional mapping of cortical circuitry through a novel combination of voltage sensitive dye
592 imaging and laser scanning photostimulation. J Neurophysiol *103*, 2301-2312.
593 Xu, X., Roby, K.D., and Callaway, E.M. (2006). Mouse cortical inhibitory neuron type that
594 coexpresses somatostatin and calretinin. J Comp Neurol *499*, 144-160.
595 Xu, X., Sun, Y., Holmes, T.C., and Lopez, A.J. (2016b). Noncanonical connections between the
596 subiculum and hippocampal CA1. J Comp Neurol *524*, 3666-3673.

597

598

599

600 **Table 1. Intrinsic physiological properties of mossy cells at different ages**

Mouse age	RMP (mV)	Rs (MΩ)	Rinput (MΩ)	Cm (pF)	Evoked spike rate (Hz)
P6-7 (N = 11)	-60.3 ± 1.7	32.6 ± 2.4	637.7 ± 74.0	70.4 ± 10.3	5.6 ± 1.1
P13-14 (N = 12)	-61.5 ± 1.1	27.2 ± 3.0	439.8 ± 37.7	111.8 ± 10.7	1.5 ± 0.6
P21-28 (N = 13)	-62.7 ± 1.6	33.4 ± 3	341.7 ± 63.5	99.9 ± 13	3.1 ± 0.9
P value	ns	ns	* P6-7 vs P13-14, 0.02 * P6-7 vs P21-28, 0.008	* P6-7 vs P13-14, 0.02 * P6-7 vs P21-28, 0.008	* P6-7 vs P13-14, 0.006

601
602 RMP, resting membrane potential; Rs, access resistance; Cm, membrane capacity; Rinput, input
603 resistance. ns, not significant for statistical comparison.

eNeuro Accepted Manuscript

Table 2. Statistics of LSPS-mapped excitatory postsynaptic current (EPSC) responses to hilar mossy cells at different ages

a. Average EPSC Integrated Input

		P6-7	P13-14	P21-28	Significance level
DG	Photostimulation Evoked Input (EI)	44.8 ± 8.4	189.9 ± 59.0	105.9 ± 12.4	* P6-7 vs P13-14, 0.05 * P6-7 vs P21-28, 0.0005
	EI per Site	3.6 ± 0.5	9.6 ± 1.5	8.3 ± 1.4	ns
	% EI	29.1 ± 6.1	62.7 ± 6.2	72.1 ± 8.4	ns
hilus	EI	18.8 ± 4.6	10.9 ± 6.6	5.3 ± 2.6	* P6-7 vs P21-28, 0.022
	EI per Site	4.1 ± 1.0	3.1 ± 1.3	1.4 ± 0.4	ns
	% EI	18.2 ± 6.3	4.8 ± 1.7	3.6 ± 1.8	ns
CA3	EI	73.1± 19.9	43.7 ± 14.6	20.7 ± 7.9	* P6-7 vs P21-28, 0.056 * P13-14 vs P21-28, 0.091
	EI per Site	3.7 ± 0.5	3.9 ± 0.7	2.5 ± 6.3	ns
	% EI	32.0 ± 5.4	22.4 ± 4.6	14.0 ± 5.3	ns

Note that the recorded cells used for this table include 12 cells (P6-7), 9 cells (P13-14) and 10 (P21-28). EI: photostimulation-evoked postsynaptic input measured from recorded neurons; %EI: the regional percentage of total evoked input; EI per site: evoked input per photostimulation.

b. Number of EPSCs recorded from mossy cells at different ages

		P6-7	P13-14	P21-28	Significance level
DG	Total Numbers	38.9 ± 7.0	70.7 ± 21.2	50.3 ± 9.3	ns
	Numbers Per Site	3.2 ± 0.5	3.9 ± 0.4	3.4 ± 0.1	ns
	% Total Events	31.2 ± 5.0	56.6 ± 6.4	56.7 ± 10.4	ns
hilus	Total Numbers	15.1 ± 3.4	4.9 ± 2.5	5.4 ± 2.7	* P6-7 vs P13-14, 0.05 * P6-7 vs P21-28, 0.0117
	Numbers Per Site	3.3 ± 0.6	1.7 ± 0.5	0.0	ns
	% Total Events	13.3 ± 4.3	5.4 ± 2.1	6.0 ± 3.0	ns
CA3	Total Numbers	60.4 ± 13.9	25.5 ± 8.4	20.5 ± 9.1	* P6-7 vs P21-28 0.0193
	Numbers Per Site	3.4 ± 0.4	2.4 ± 0.3	1.7 ± 0.3	ns
	% Total Events	33.4 ± 5.8	26.2 ± 4.7	23.1 ± 10.9	ns

eNeuro Accepted Manuscript

635 **c. Rise time, time constants, and onset latency of EPSC**
636

		P6-7	P13-14	P21-28	Significance level
DG	Rise time(ms)	2.4 ± 0.12	2.6 ± 1.3	2.5 ± 0.1	ns
	Time Constant (ms)	4.2 ± 0.2	4.2± 0.3	5.0 ± 0.6	ns
	Latency (ms)	50.5 ± 5.6	46.2 ± 6.7	42.1 ± 4.8	ns
hilus	Rise time(ms)	2.3 ± 0.2	2.9 ± 0.6	2.2 ± 0.2	ns
	Time Constant (ms)	6.7 ± 1.0	5.7 ± 0.5	6.2 ± 1.5	ns
	Latency (ms)	46.9 ± 4.9	59.1 ± 7.3	39.2 ± 9.1	ns
CA3	Rise time(ms)	2.4 ± 0.1	3.1 ± 0.1	2.7 ± 0.3	* P6-7 vs P13-14, 0.004 * P13-14 vs P21-28, 0.04
	Time Constant (ms)	7.2 ± 0.3	4.4 ± 0.3	3.4 ± 0.9	ns
	Latency (ms)	44.1 ± 3.0	51.0 ± 7.4	47.2 ± 10.3	ns

637

Table 3. Statistics of LSPS-mapped inhibitory postsynaptic current (IPSC) responses to hilar mossy cells at different ages

a. Average IPSC Integrated Input

		P6-7	P13-14	P21-28	Significance level
DG	Photostimulation Evoked Inout (EI)	68.5 ± 24.0	490.7 ± 100.6	195.7 ± 37.0	* P6-7 vs P13-14, 0.005 * P6-7 vs P21-28, 0.0001
	EI Per Site	3.9 ± 0.9	12.8 ± 1.4	6.6 ± 0.8	ns
	% EI	31.2 ± 5.5	62.3 ± 5.0	64.8 ± 3.6	ns
hilus	EI	28.1 ± 8.8	132.2 ± 35.2	31.6 ± 4.8	* P6-7 vs P13-14, 0.002 *P13-14 VS P21-28 0.004
	EI Per Site	4.7 ± 1.3	10.7 ± 2.1	4.7 ± 0.50	ns
	% EI	18.2 ± 3.9	14.9 ± 3.0	17.9 ± 4.5	ns
CA3	EI	77.1 ± 20.5	150.6 ± 30.4	51.8 ± 13.6	* P6-7 vs P13-14, 0.05 *P13-14 VS P1-28 0.002
	EI Per Site	4.3 ± 0.8	10.8 ± 2.1	4.2 ± 0.9	ns
	% EI	40.5 ± 6.2	18.5 ± 2.5	11.7 ± 2.9	ns

638 Note that the recorded cells used for this table include 10 cells (P6-7), 7 cells (P13-14) and 16 (P21-28).
639 EI, EI per site, and %EI are the same as in Table 2a.

640 **b. Number of IPSCs recorded from mossy cells at different ages**
641

		P6-7	P13-14	P21-28	Significance level
DG	Total Numbers	32.6 ± 11.7	105.3 ± 21.1	80.4 ± 14.3	* P6-7 vs P13-14, 0.01 * P6-7 vs P21-28, 0.003
	Numbers Per Site	2.0 ± 0.4	3.7 ± 0.4	2.9 ± 0.2	ns
	% Total Events	31.1 ± 5.6	56.3 ± 4.8	63.1 ± 3.2	ns
hilus	Total Numbers	15.2 ±4.2	35.4 ± 9.8	17.2 ± 2.4	* P6-7 vs P13-14, 0.05 * P13-14 vs P21-28, 0.02
	Numbers Per Site	2.6 ± 0.6	3.4 ± 0.6	2.6 ± 0.2	ns
	% Total Events	19.3 ± 3.9	17.1 ± 2.6	19.1 ± 4.0	ns
CA3	Total Numbers	36.2 ± 9.1	44.3 ± 13.2	21.4 ± 4.9	ns
	Numbers Per Site	2.2 ± 0.36	3.0 ± 0.5	1.8 ± 0.3	ns
	% Total Events	39.3 ± 6.4	19.9 ± 2.7	11.9 ± 2.8	ns

eNeuro Accepted Manuscript

eNeuro Accepted Manuscript

642
643 **c. Rise time, time constants, and onset latency of IPSCs**
644

		P6-7	P13-14	P21-28	Significance level
DG	Rise time(ms)	4.1 ± 0.2	4.0 ± 0.2	4.4 ± 0.2	ns
	Time Constant (ms)	9.3 ± 0.1	7.7 ± 0.8	7.4 ± 0.3	*P6-7 vs P21-28, 0.02
	latency(ms)	57.1 ± 2.2	34.8 ± 1.6	40.2 ± 2.5	* P6-7 vs P13-14, 0.0003 * P6-7 vs P21-28, 0.00009 P13-14 vs P21-28, 0.07
hilus	Rise time(ms)	4.6 ± 0.3	4.4 ± 0.3	4.8 ± 0.2	ns
	Time Constant (ms)	7.3 ± 0.0	7.7 ± 1.0	9.4 ± 0.8	ns
	latency(ms)	39.3 ± 6.5	28.7 ± 4.3	33.0 ± 2.9	ns
CA3	Rise time(ms)	4.4 ± 0.3	3.5 ± 0.4	4.5 ± 0.2	* P6-7 vs P13-14, 0.05 * P13-14 vs P21-28, 0.03
	Time Constant (ms)	8.8 ± 0.1	7.0 ± 0.8	8.6 ± 0.6	ns
	Latency (ms)	61.5 ± 6.2	34.0 ± 4.5	35.8 ± 2.5	* P6-7 vs P13-14, 0.008 * P6-7 vs P21-28, 0.003

645

eNeuro Accepted Manuscript

646 **Figure legends**

647 **Figure 1. Targeted recordings of hilar mossy cells. A.** Horizontal hippocampal slices are
648 acutely prepared from GAD-Cre: Ai9 tdTomato double transgenic mice and are visualized under
649 a 4x objective. Whole-cell recordings are made from mossy cells in the dentate gyrus (green
650 circle). Scale bar=250uM. **B.** Mossy cells, as shown with a 60x objective, are first identified by
651 their lack of tdTomato fluorescence (under the pipette, white square) in the hilar region of GAD-
652 Cre: Ai9 mice. Scale bar=50uM. **C.** Morphology of recorded mossy cells (white arrows), which
653 are injected with biocytin (green), demonstrates multipolar soma and thick dendrites with thorny
654 excrescences. Scale bar=50uM. **D.** Mossy cells have regular/adapting spiking in response to
655 current injection (horizontal black line) through the patch pipette.

656

657 **Figure 2. Developmental changes in intrinsic physiological and morphological properties**
658 **of mossy cells. A.** Example responses to current injection (horizontal lines) in example mossy
659 cells recorded from P7, P14, and P21 mice. **B-C.** Example morphology of biocytin-labeled
660 mossy neurons (green) and surrounding DAPI stained tissue (blue) at P7, P14, and P21. The
661 labeled neurons in the P7 mouse had proximal dendrites with branches penetrated into the
662 fascia dentate (arrows for P7 mouse in B), and were relatively smooth (image shown in C).
663 While neurons recorded in P14 and P21 mice have obvious thorny excrescence (arrows in C)
664 on proximal dendrites. Scale bar=250uM in B. Scale bar=25uM in C. All labeled neurons had
665 large, multipolar somata and thick thorny proximal dendrites. A neuron (circle in B) in the P14
666 mouse is in CA3. **D.** The input resistance (Left, measured in MΩ) decreased with age from P6-7
667 to P13-14, and P21-28. The membrane capacity (Middle, measured in pF), is the capacitance of
668 the cell membrane, and increased with age from P6-7 to P13-14, and P21-28. The spike rate
669 (Right, measured in Hz), is the number of evoked spikes in response to current injection of 100
670 pA during recording, and decreased with age from P6-7 to p13-14.

671

eNeuro Accepted Manuscript

672 **Figure 3. LSPS mapping and data analysis. A.** A horizontal hippocampal slice under a 4x
673 objective with a patched neuron (red circle) and laser stimulation sites overlaid (cyan asterisks).
674 **B.** Raw signal traces recorded from the patched neuron during laser stimulation. **C.** Examples of
675 a direct response (top green trace) which has a large amplitude and a short response latency,
676 and synaptic responses (bottom red) which have smaller amplitudes and longer latencies. **D-**
677 **F.** Synaptic responses were detected and extracted using automatic software processing (Shi et
678 al, 2010). Input amplitude, as defined by the distance of the baseline to the peak of the EPSC
679 (D), the number of evoked synaptic events, as defined by the number of EPSCs elicited per
680 laser pulse (E), and the number of spontaneous events (F) were plotted in heat maps.
681
682 **Figure 4. Spatial precision of LSPS mapping for neurons in the DG, hilus, and CA3c. A-B.**
683 Excitation profile of a recorded DG granule cell from a mouse hippocampal slice. The excitation
684 profile shows the spatial distribution of uncaging sites that produce action potentials. The cell is
685 held in current clamp mode. The cyan asterisks in A are the stimulation sites (75 μm spacing).
686 The evoked action potentials were restricted to a small region (yellow square). Raw signal
687 traces within the yellow square are shown in B. **C-D.** Excitation profile of a hilar mossy cell from
688 a mouse hippocampal slice (100 μm spacing). **E-F.** Excitation profile of CA3 pyramid cells from
689 mouse hippocampal slice (100 μm spacing). Excitation profiles show no spike-evoking sites
690 distal from the perisomatic area of the recorded neuron, demonstrating that LSPS maps
691 represent input from monosynaptic connections.
692

eNeuro Accepted Manuscript

693 **Figure 5. Anatomical map of excitatory input to mossy cells across developmental ages.**
694 **A.** Strength of excitatory input (input amplitudes) at P7, P14, and P24 for a representative
695 mossy cell. **B**. Frequency of EPSC events (number of evoked synaptic events per second) for a
696 representative mossy cell. **C-D**. Summed (averaged) amplitude of excitatory inputs to mossy
697 cells. We recorded from 12, 9, and 10 cells from P6-7, P13-14 and P21-28 mice, respectively.
698 In the left two panels of C, the y-axis indicates input strength. In the right panel in D, the y-axis
699 shows the ratio of input strengths.
700
701
702 **Figure 6. Anatomical map of inhibitory input to mossy cells across developmental ages**.
703 **A.** Strength of inhibitory input amplitude at P7, P14 and P24 for a representative mossy cell. **B.**
704 Frequency of IPSC events (number of evoked synaptic events per second) for a representative
705 mossy cell. **C-D.** Summed (averaged) amplitude of inhibitory inputs to mossy cells. We mapped
706 10, 7, and 16 cells from P6-7, P13-14, and P21-28 mice, respectively. In the left two panels of
707 C, the y-axis indicates input strength. In the right panel in D, the y-axis shows the ratio of input
708 strengths.
709

eNeuro Accepted Manuscript

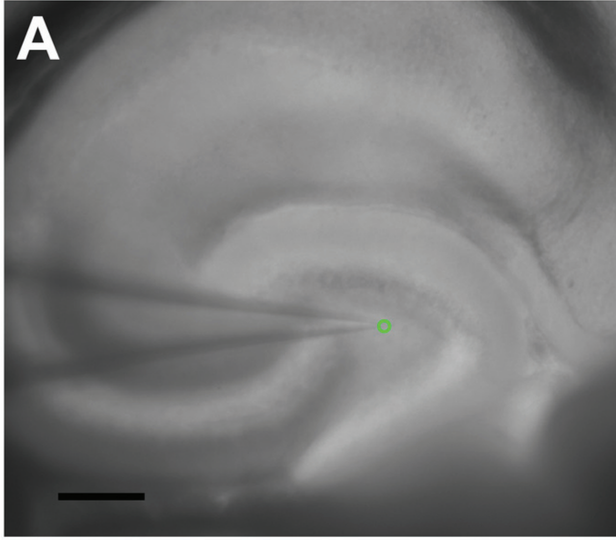

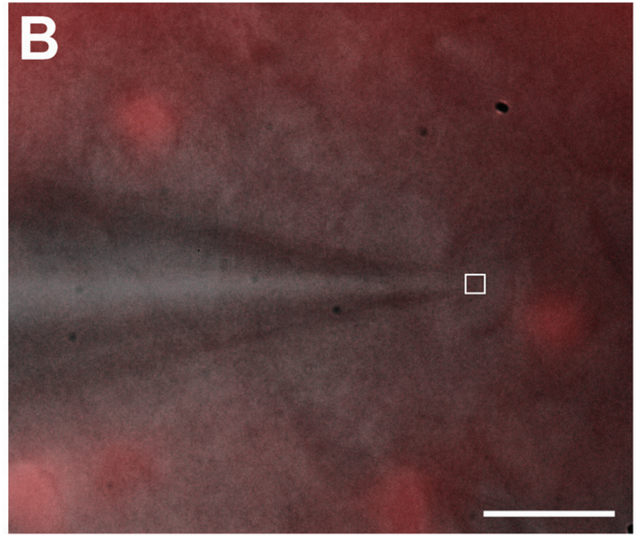

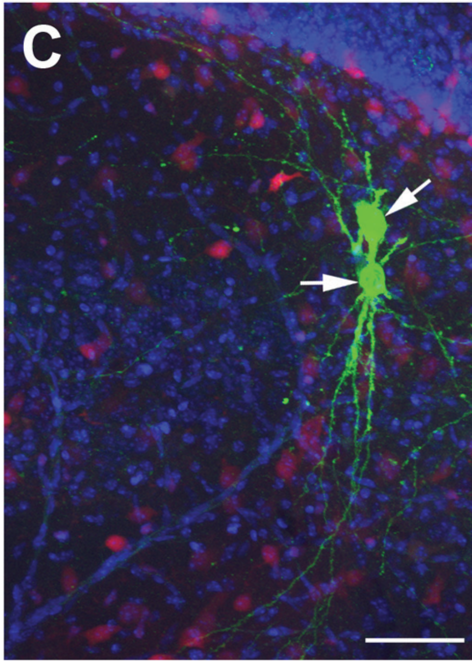

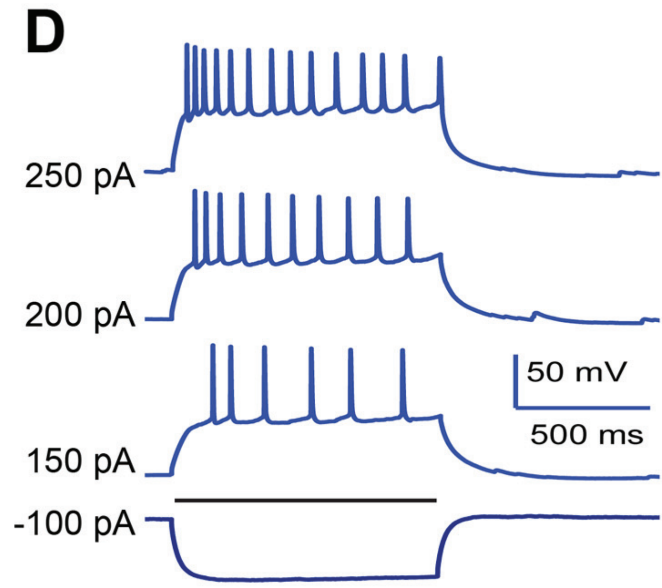

eNeuro Accepted Manuscript

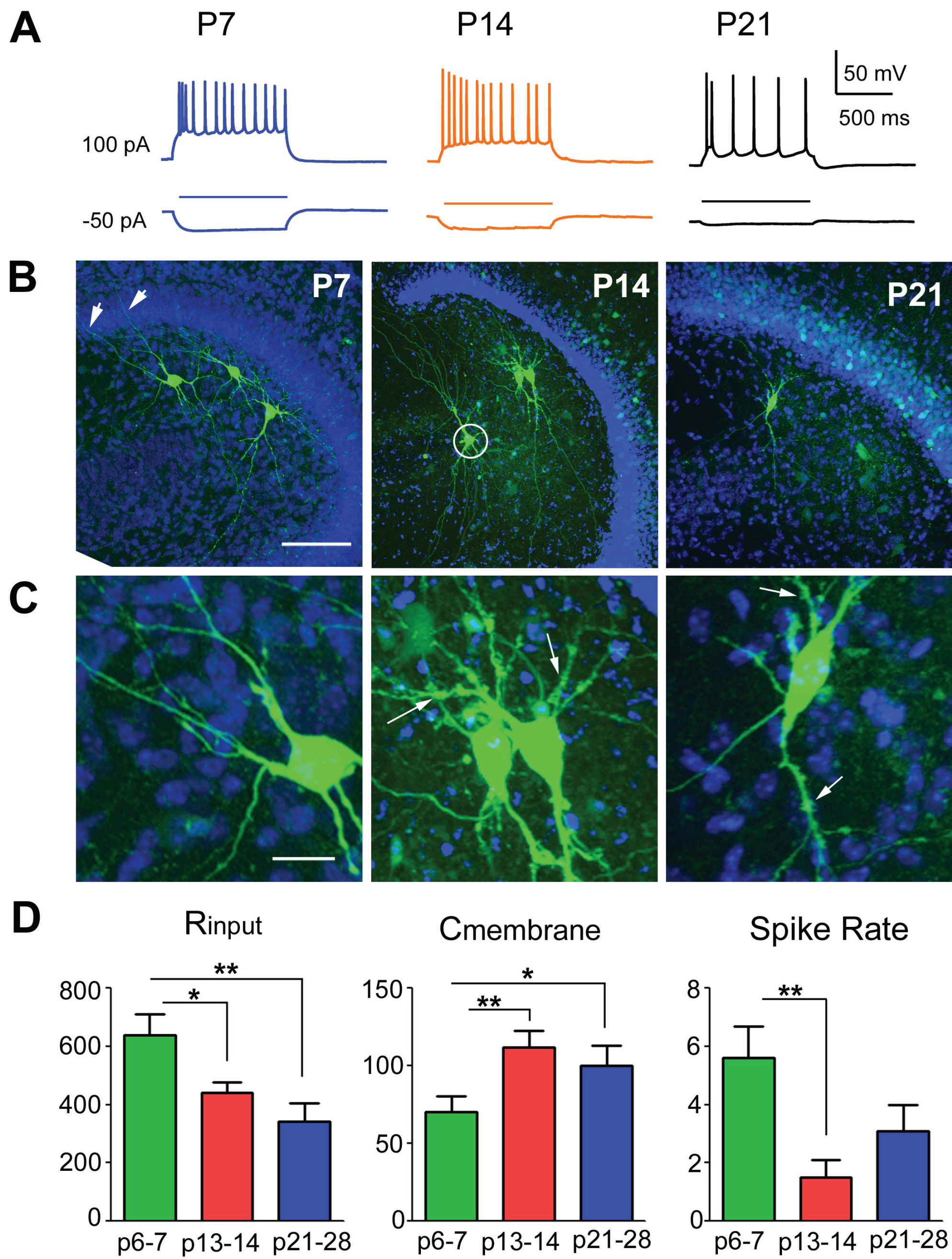

eNeuro Accepted Manuscript

A

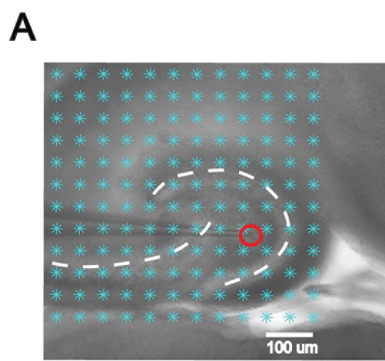

B

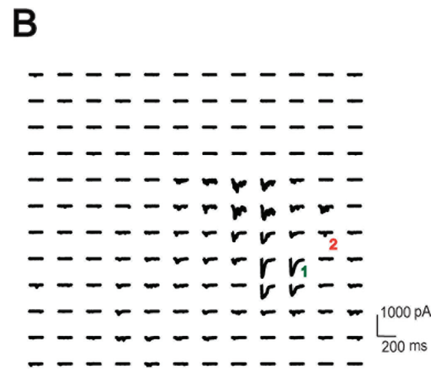

C

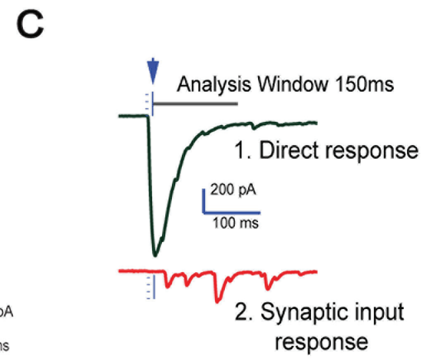

D

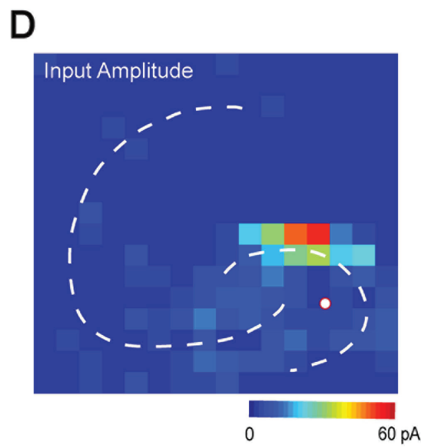

E

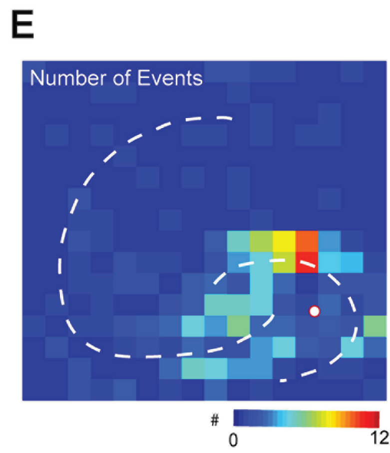

F

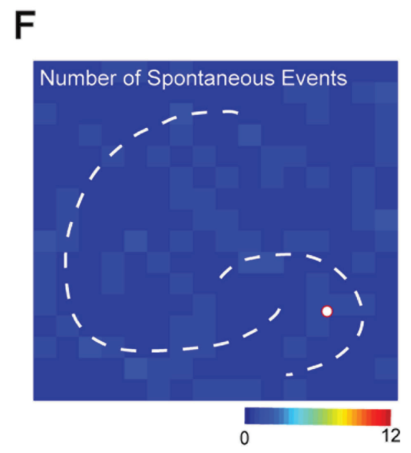

eNeuro Accepted Manuscript

A.

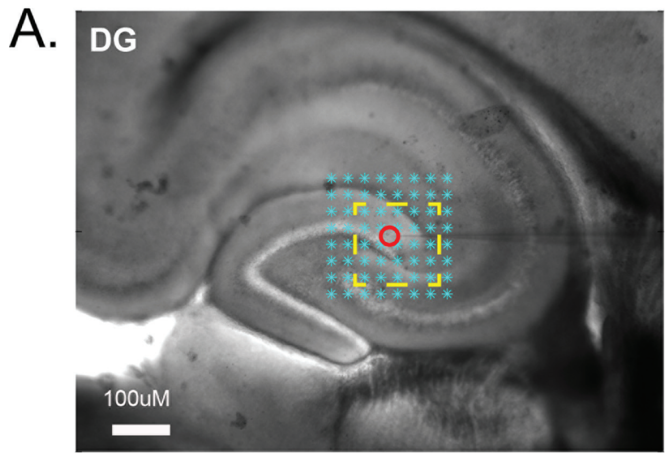

B.

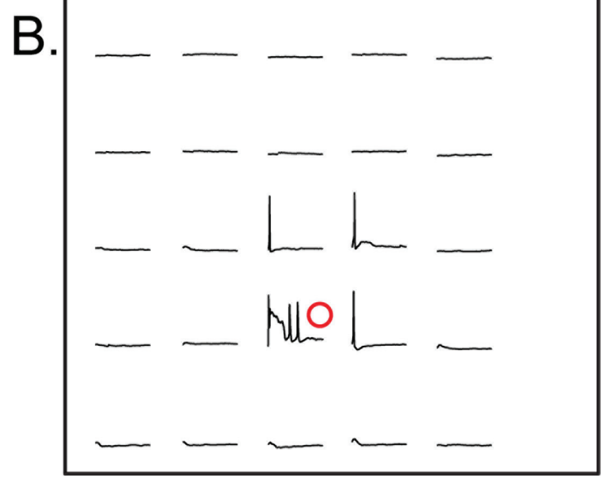

C.

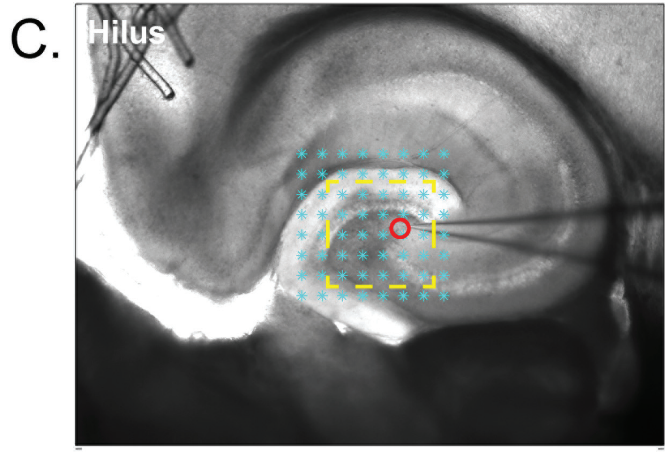

D.

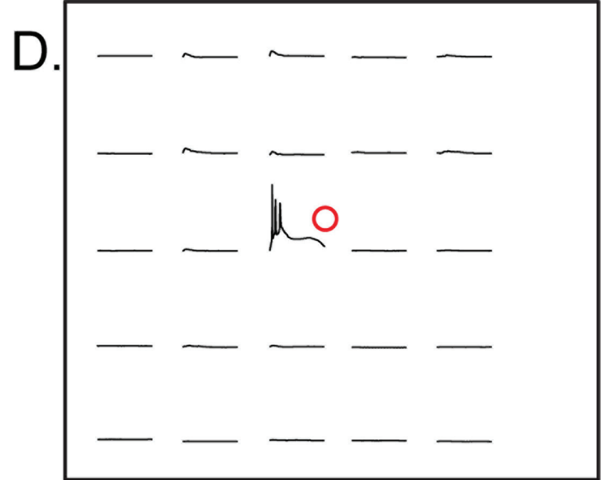

E.

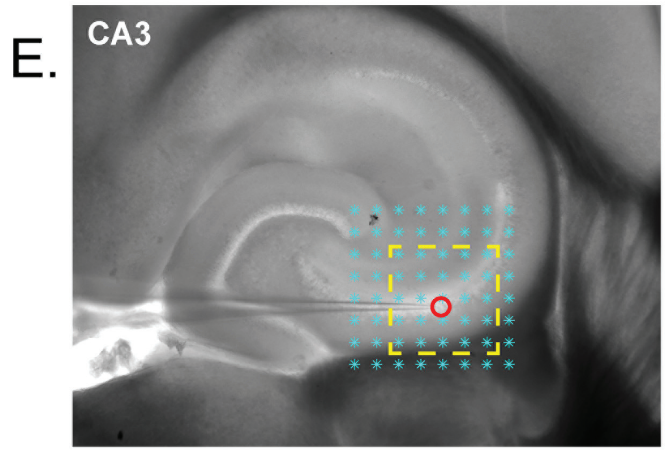

F.

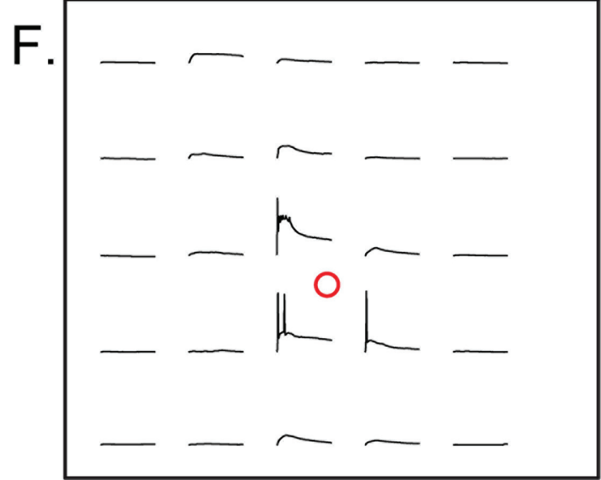

eNeuro Accepted Manuscript

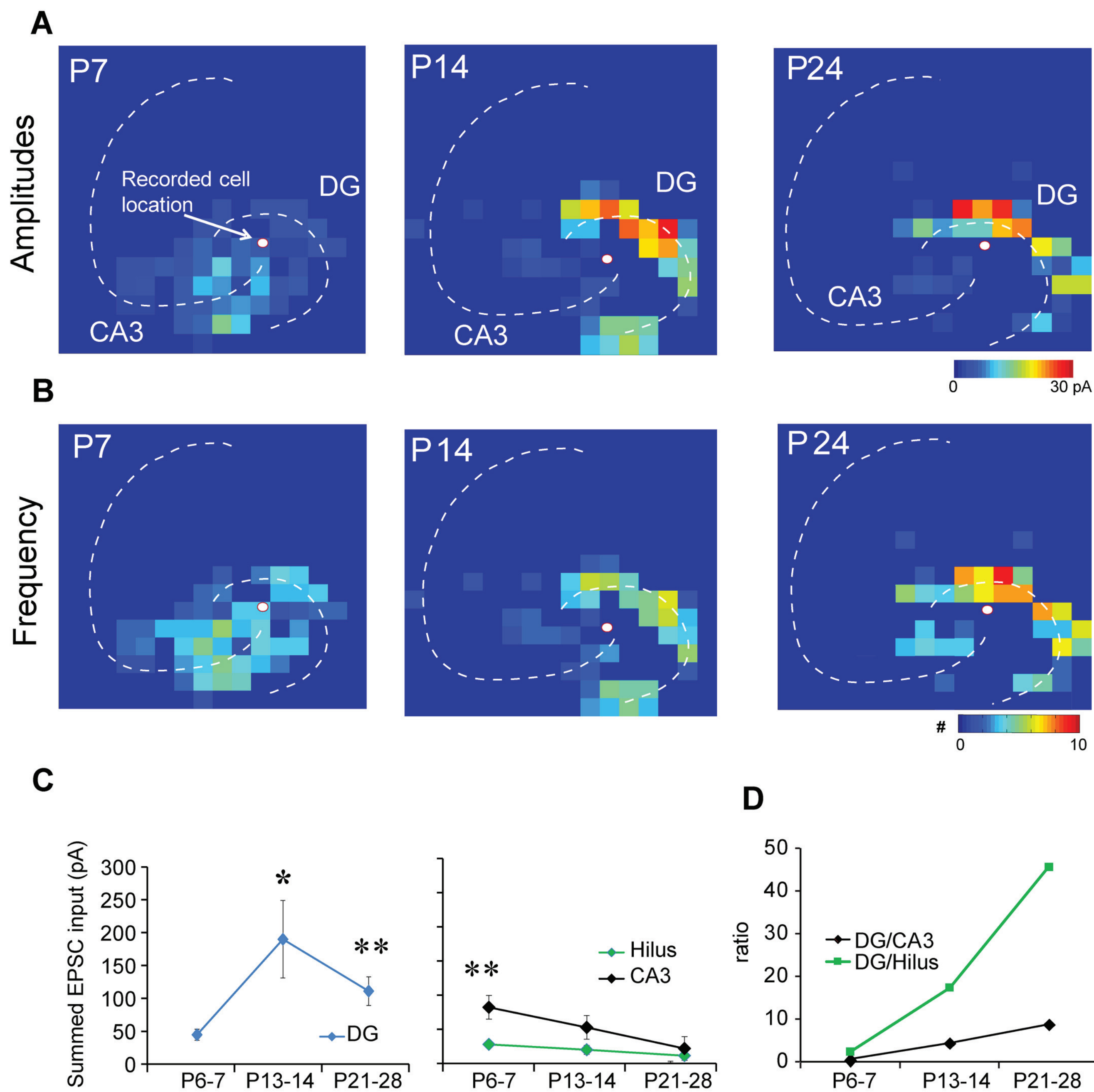

eNeuro Accepted Manuscript